Homotopy perturbation technique for improving solutions of large quadratic eigenvalue problems: Application to friction-induced vibration

Jérémy Sadet, Franck Massa, Thierry Tison, Isabelle Turpin, Bertrand Lallemand, El-Ghazali Talbi

Homotopy perturbation technique for improving solutions of large quadratic eigenvalue problems: Application to friction–induced vibration

Article *in* Mechanical Systems and Signal Processing · December 2020

DOI: 10.1016/j.ymssp.2020.107492

CITATIONS
0

READS
14

6 authors, including:

Jérémy Sadet
Université Polytechnique Hauts-de-France
1 PUBLICATION **0** CITATIONS
SEE PROFILE

Franck Massa
Université Polytechnique Hauts-de-France
39 PUBLICATIONS **395** CITATIONS
SEE PROFILE

Thierry Tison
Université Polytechnique Hauts-de-France
61 PUBLICATIONS **625** CITATIONS
SEE PROFILE

Isabelle Turpin
Université Polytechnique Hauts-de-France
13 PUBLICATIONS **112** CITATIONS
SEE PROFILE

Homotopy perturbation technique for improving solutions of large quadratic eigenvalue problems: Application to friction-induced vibration

Jérémy SADET[a,c], Franck MASSA[a], Thierry TISON[a], Isabelle TURPIN[b], Bertrand LALLEMAND[a], El-Ghazali TALBI[c]

[a] *Hauts-de-France Polytechnic University, LAMIH UMR CNRS 8201, F-59313 Valenciennes*
[b] *Hauts-de-France Polytechnic University, LMI, F-59313 Valenciennes*
[c] *Team BONUS, University of Lille, INRIA Lille Nord Europe, France*

Abstract

This paper puts forward a projection technique for accurately calculating solutions of large Quadratic Eigenvalue Problem. The aim here is to stabilize the complex eigensolutions whilst reducing residual errors, especially when considering significant damping contribution or asymmetric stiffness matrices. Hence, more confident results can be obtained in the frequency band of interest. To achieve this, high order modes, calculated using the homotopy perturbation technique, are introduced in the projection step of the classical method. This numerical proposal is a generalization of the classical projection, based only on normal modes of the associated undamped problem. To evaluate the efficiency of the suggested method, a finite element application dedicated to a friction-induced vibration problem is investigated.

Keywords: Quadratic Eigenvalue Problem; Homotopy; Perturbation; Projection; Nonlinear vibration; Friction-induced vibration

1. Introduction

In mechanical engineering, the modal analysis of large undamped structures discretized by the Finite Element Method (FEM) is performed using the Generalized Eigenvalue Problem (GEP) from the definition of mass and stiffness matrices. However, when damping is of main interest or in other applications, such as vibroacoustics, fluid dynamics or friction-induced vibration problems, solutions are the results of a Quadratic Eigenvalue Problem (QEP) for which a complete and practical survey can be found in [1]. In this case, large discrete models require a projection onto a relevant subspace. In modal analysis, the classical method uses a basis built with a set of eigenvectors of the associated undamped model. For the complex applications cited above, this basis is not generally optimal and can lead to significant errors. For example, for a friction-induced vibration problem, one of the reasons for potential errors is that the coupled normal modes are a poor representation of the model dynamics subjected to friction. Many methods (sub structuring, component mode synthesis, condensation, reanalysis techniques, etc.) are based on the construction of reduced models by means of projection on a basis of displacements. It is known that these methods provide accurate results when properly used, or in other words, when the reduced subspace spanned by the columns of the rectangular projection matrix represents a close approximation of the full order model [2]. It is also known that increasing the subspace size with additional vectors of the same type slowly improves the solutions and is not interesting for numerical cost reasons.

It is thus more interesting to investigate other categories of subspaces already used in other contexts such as Taylor series [3], perturbations techniques [4, 5, 6, 7], Padé approximant [8, 9] or Homotopy Perturbation Method (HPM) introduced by He [10]. At first, the HPM was used in the literature to calculate nonlinear solutions for different applications. Duigou et al. [11] have associated homotopy, asymptotic numerical techniques and Padé approximants to investigate the vibrations of damped sandwich structures whereas Boumediene et al. [12] have developed a reduction method for solving the complex nonlinear eigenvalue

problem regarding viscoelastic structures. Sun et al. [13] have provided numerical solutions for sound-propagation computations using the homotopy method. Next, Lee et al. [14] have searched for asymptotic solutions of nonlinear problems with the HPM to yield natural frequencies. For vibroacoustic applications, Claude et al. [15] put forward a numerical method to solve non-symmetric eigenvalue problems and discussed of the efficiency of eigensolvers depending on Taylor or asymptotic expansions in [16]. Recently, the same authors have suggested computing damped eigenfrequencies and modes with a high order Newton solver, based on homotopy and perturbation techniques [17]. Secondly, several authors have considered the HPM to estimate modified solutions of a perturbed problem by reanalysis or by Reduced Order Model (ROM). Indeed, Sliva et al. [18] suggested solving the new eigenvalue problem with the combination of a homotopy transformation and the perturbation method. Next, Li et al. [19] have worked on the calculation of complex eigenpairs of modified asymmetric systems as a way of creating a Campbell diagram of the modified rotor system. Massa et al. [20] have integrated two-level homotopy techniques to estimate instabilities of a friction-induced vibration problem. Do et al. [21] used the HPM to reanalyse modal bases of modified components of a mechanical system before using them in the component modal synthesis. More recently, Massa et al. [22] have defined a ROM for a linear modal analysis by considering a projection basis made of high order perturbed eigenvectors.

In this paper, we suggest using the HPM to compute QEP high order modes. These modes are used to build an enriched projection basis before solving the reduced QEP resulting from a dynamic analysis of structures discretized by the FEM. With the classical method, variations of the complex eigensolutions values are often observed when the number of normal modes in the projection basis is modified. With the suggested method, the aim is to stabilize the results of the QEP while reducing the residual errors. The quality of the eigensolutions is thus improved and results are proven to be more accurate.

Section 2 reviews the QEP and its classical way of resolution. Section 3 generalizes the classical projection basis to higher order eigenvectors. Next, section 4 presents an example of a friction-induced vibration problem. Finally, section 5 offers a summary of our conclusions for this novel strategy.

2. Quadratic Eigenvalue Problem definition

Although some problems in structural dynamics are defined by non-symmetric matrices, only the right quadratic eigenvalue problem will be discussed in the sequel. Let us consider the QEP given by Eq.(1) :

$$\left(\mathbf{K} + s_i\mathbf{C} + s_i^2\mathbf{M}\right)\boldsymbol{\psi}_i = \mathbf{0} \tag{1}$$

where s_i and $\boldsymbol{\psi}_i$, are respectively the i^{th} eigenvalue and the i^{th} right eigenvector.

$\mathbf{M}$, $\mathbf{C}$ and $\mathbf{K}$ are respectively the [N $\times$ N] mass, damping and stiffness matrices of the discretized mechanical system, with N representing the number of Degree Of Freedom (DOF). The case where the three matrices are Hermitian positive definite, or positive semidefinite for $\mathbf{C}$ and $\mathbf{K}$, corresponds to a structure modeled with viscous damping. This QEP corresponds also to a damped mechanical system where components are coupled by normal contact entries. Eigenvalues of such problems are real or complex conjugate and come in pairs. For gyroscopic systems, $\mathbf{M}$ and $\mathbf{K}$ are Hermitian, with $\mathbf{M}$ definite positive, and $\mathbf{C}$ skew Hermitian ($\mathbf{C} = -\mathbf{C}^H$, with $\mathbf{C}^H$ the conjugate transpose of $\mathbf{C}$). In this case, eigenvalues are purely imaginary. When the mechanical system is subjected to friction (such as friction-induced vibration problems), tangential loads induced a non-symmetric stiffness matrix resulting from the tangential coupling. Even if damping is not considered, complex solutions of the latter QEP can reveal positive real parts which make it possible to determine the stability of the system. Other types of problems such as vibroacoustic, fluid mechanics studies, control theory in the field of automatic and even numerical optimization can also be reduced to a QEP. For a complete description of these applications, the interested readers can refer to the paper of Tisseur et al. [1]. The suggested algorithm can be applied to the aforementioned problems. In this paper, we will specifically illustrate the case of a friction-induced vibration problem because the friction effect

can introduce large errors in the evaluation of complex eigensolutions. The well-known global QZ algorithm [23] is efficient for solving the QEP of small discrete numerical systems (typically when N<1000). For large Finite Element (FE) models, a projection onto a $\mathbf{T}$ subspace is needed to build a reduced approximate modal problem that is compatible with the QZ algorithm. In practice, the subspace $\mathbf{T}$ is made up of the first normal modes of the associated conservative system given by Eq.(2) :

$$\left(\mathbf{K} - \omega_i^2 \mathbf{M}\right) \boldsymbol{\phi}_i = \mathbf{0} \tag{2}$$

where ω_i and $\boldsymbol{\phi}_i$, are respectively the i^{th} natural circular frequency and the i^{th} normal mode.

Considering both the projection basis and the linearization of the QEP (according to the definition in [1]), one can obtain a GEP of the second companion form given by Eq.(3).

$$\mathbf{A}\mathbf{u}_i = s_i \mathbf{B}\mathbf{u}_i \tag{3}$$

where $\mathbf{A} = \begin{bmatrix} -\mathbf{T}^T\mathbf{K}\mathbf{T} & \mathbf{0} \\ \mathbf{0} & \mathbf{T}^T\mathbf{M}\mathbf{T} \end{bmatrix}$, $\mathbf{B} = \begin{bmatrix} \mathbf{T}^T\mathbf{C}\mathbf{T} & \mathbf{T}^T\mathbf{M}\mathbf{T} \\ \mathbf{T}^T\mathbf{M}\mathbf{T} & \mathbf{0} \end{bmatrix}$, $\mathbf{u}_i = \begin{pmatrix} \boldsymbol{q}_i \\ s_i^* \boldsymbol{q}_i \end{pmatrix}$ and $\boldsymbol{\psi}_i^* = \mathbf{T}\boldsymbol{q}_i$, s_i^* and $\boldsymbol{\psi}_i^*$ are approximations of the QEP eigensolutions in Eq.(1).

The above strategy is common and largely implemented in commercial finite element softwares. In most of the practical problems, particularly the modal analysis with viscous damping, solutions of Eq.(3) are very satisfactory. When studying the stability of rubbing systems, some discrepancies arise which could alter the judgment of the behaviour of the mechanical system. These errors can be reduced by adding appropriate modes calculated from the HPM presented in the next section.

3. Homotopy resolution of the QEP equation

Many physical phenomena are modelled using systems of nonlinear differential equations, which is a straightforward way to describe their behaviours. As these equations are generally difficult to solve, many alternative and powerful methods have been developed over the last few years, for instance, the decomposition method [24], the variational iteration method [25, 26], the HPM [27], Generalized Homotopy Method (GHM) [28] and the differential transform method [29]. Each method is limited to a special class of integro-differential equations and short reviews are available for different applications [30, 31]. The Homotopy Perturbation Method, used in this paper to build the projection space, has been improved from 2000 to present days [32, 33, 34] and applied to study different problems integrating nonlinear oscillators [35, 36].
The following section details an implementation of the homotopy perturbation technique for solving a QEP problem where matrices can be asymmetric.

3.1. Homotopy Perturbation technique

Solutions of non-linear equations can be obtained using the HPM which combines the standard homotopy in topology and the perturbation technique. The idea behind the HPM is to separate the linear and non-linear parts of the problem and to introduce an embedding parameter ε to highlight the non-linearity. Assuming that the embedding parameter is small, approximate solutions of the non-linear equations can be written as a power series in ε.

Considering the general case of the QEP, the basic idea of the suggested methodology is to introduce the HPM in two ways. The first one concerns the symmetric and asymmetric contributions of the mass and stiffness matrices. The decomposition in Eq.(4) represents the symmetric contribution, the S index, and the asymmetric contribution, the A index. Decomposition is presented here for both mass and stiffness matrices for the sake of generality but the asymmetric contribution can easily be suppressed in the case of a purely symmetric matrix.

$$\begin{aligned}\mathbf{M} &= \mathbf{M}_S + \varepsilon\mathbf{M}_A \\ \mathbf{K} &= \mathbf{K}_S + \varepsilon\mathbf{K}_A\end{aligned} \tag{4}$$

where $\mathbf{M}_S$, $\mathbf{M}_A$, $\mathbf{K}_S$, $\mathbf{K}_A$ stand for the symmetric and asymmetric decomposition of the mass and stiffness matrices, respectively.

The second decomposition is related to damping which is completely considered as a non-linear part of Eq.(1). The decomposition of the damping matrix $\mathbf{C}$ is then different as all entries are considered to be asymmetric contributions such as :

$$\mathbf{C} = \varepsilon\mathbf{C}_A \tag{5}$$

According to the HPM, the i^{th} eigensolution of Eq.(1) is developed as a power series in ε with a nominal term, the (0) index, and higher order contributions, indexed by (n), such as :

$$\begin{aligned}s_i &= s_i^{(0)} + \varepsilon s_i^{(1)} + \ldots + \varepsilon^n s_i^{(n)} + \ldots + \varepsilon^d s_i^{(d)} \\ \boldsymbol{\psi}_i &= \boldsymbol{\psi_i}^{(0)} + \varepsilon\boldsymbol{\psi}_i^{(1)} + \ldots + \varepsilon^n\boldsymbol{\psi}_i^{(n)} + \ldots + \varepsilon^d\boldsymbol{\psi}_i^{(d)}\end{aligned} \tag{6}$$

where d is truncation order.

Substituting Eq.(4), Eq.(5) and Eq.(6) into Eq.(1), the QEP is rewritten as follows :

$$\begin{aligned}&\Big[(\mathbf{K}_S + \varepsilon\mathbf{K}_A) + \left(s_i^{(0)} + \varepsilon s_i^{(1)} + \ldots + \varepsilon^n s_i^{(n)} + \ldots + \varepsilon^d s_i^{(d)}\right)\varepsilon\mathbf{C}_A \\ &\quad + \left(s_i^{(0)} + \varepsilon s_i^{(1)} + \ldots + \varepsilon^n s_i^{(n)} + \ldots + \varepsilon^d s_i^{(d)}\right)^2 (\mathbf{M}_S + \varepsilon\mathbf{M}_A)\Big] \\ &\qquad \left(\boldsymbol{\psi}_i^{(0)} + \varepsilon\boldsymbol{\psi}_i^{(1)} + \ldots + \varepsilon^n\boldsymbol{\psi}_i^{(n)} + \ldots + \varepsilon^d\boldsymbol{\psi}_i^{(d)}\right) = 0\end{aligned} \tag{7}$$

From Eq.(7), it is possible to identify the n^{th} homotopy order and the high order vectors associated with that order. The next subsections describe the form of the nominal (0^{th} order), the 1^{st} order and any n^{th} order of the high order vectors.

3.2. Identification of the nominal terms

Terms of the 0^{th} order are simply obtained setting $\varepsilon = 0$ in Eq.(7) leading to a GEP of the form :

$$\left(\mathbf{K}_S + {s_i^{(0)}}^2\mathbf{M}_S\right)\boldsymbol{\psi}_i^{(0)} = \mathbf{0} \tag{8}$$

where $s_i^{(0)}$ is the i^{th} nominal eigenvalue and $\boldsymbol{\psi}_i^{(0)}$ is the i^{th} nominal eigenvector.

Eq.(8) has no asymmetric contributions. Moreover, substituting $s_i^{(0)}$ by $j\omega_i^{(0)}$ (with j, the imaginary unit), the problem is equivalent to the linear eigenvalue problem in Eq.(2) and can be computed with a classical eigenvalue algorithm, for example a Lanczos solver, with eigenvectors normalized according to the mass matrix such as :

$$\boldsymbol{\psi}_i^{(0)T}\mathbf{M}_S\boldsymbol{\psi}_i^{(0)} = 1 \tag{9}$$

3.3. Identification of the 1^{st} order terms

Considering only the 1^{st} order terms, Eq.(7) is rewritten as followed :

$$\begin{aligned}\left(\mathbf{K}_S + {s_i^{(0)}}^2\mathbf{M}_S\right)\boldsymbol{\psi}_i^{(1)} + \left(2s_i^{(0)}\mathbf{M}_S\boldsymbol{\psi}_i^{(0)}\right)s_i^{(1)} + \mathbf{G}_i^{(1)} = 0 \\ \mathbf{G}_i^{(1)} = \left(\mathbf{K}_A + s_i^{(0)}\mathbf{C}_A + {s_i^{(0)}}^2\mathbf{M}_A\right)\boldsymbol{\psi}_i^{(0)}\end{aligned} \tag{10}$$

Premultiplying (10) by ${\boldsymbol{\psi}_i^{(0)}}^T$ and considering Eq.(8), the 1^{st} order eigenvalue is written as :

$$s_i^{(1)} = \frac{-{\boldsymbol{\psi}_i^{(0)}}^T\mathbf{G}_i^{(1)}}{2s_i^{(0)}} \tag{11}$$

Eq.(10) can be rewritten to be of the form of Eq.(8) with a non-zero right member :

$$\left(\mathbf{K}_S + s_i^{(0)}\mathbf{M}_S\right)\boldsymbol{\psi}_i^{(1)} = \mathbf{F}_i^{(1)} \tag{12}$$

where $\mathbf{F}_i^{(1)} = -\left(2s_i^{(0)}\mathbf{M}_S\boldsymbol{\psi}_i^{(0)}\right)s_i^{(1)} - \boldsymbol{G}_i^{(1)}$

Unfortunately, $\left(\mathbf{K}_S + {s_i^{(0)}}^2\mathbf{M}_S\right)$ is not invertible. Another equation is needed to determine $\boldsymbol{\psi}_i^{(1)}$.

The chosen solution follows Wang's proposal for the calculation of eigenvector derivatives in [37]. The idea is to express each perturbed eigenvector as a linear combination of the 0^{th} order eigenvectors $\boldsymbol{\psi}_i^{(0)}$, i.e normal modes, of the system. For the 1^{st} order eigenvector, the linear combination reads:

$$\boldsymbol{\psi}_i^{(1)} = \sum_{k=1}^{N} c_k^{(1)}\boldsymbol{\psi}_k^{(0)} \tag{13}$$

In practice, the number m of available normal modes is lower than N. A common solution is to complete the development with a static correction term $\boldsymbol{\Gamma}_i^{(1)}$. The linear combination Eq.(13) is then rewritten as:

$$\begin{aligned}\boldsymbol{\psi}_i^{(1)} &= \sum_{k=1}^{m} c_k^{(1)}\boldsymbol{\psi}_k^{(0)} + \boldsymbol{\Gamma}_i^{(1)} \\ \boldsymbol{\Gamma}_i^{(1)} &= \mathbf{K}_S^{-1}\mathbf{F}_i^{(1)} - \sum_{k=1}^{m}\frac{\boldsymbol{\psi}_k^{(0)}\boldsymbol{F}_i^{(1)}}{{w_k^{(0)}}^2}\boldsymbol{\psi}_i^{(0)}\end{aligned} \tag{14}$$

For $i \neq k$, coefficients $c_k^{(1)}$ are calculated with Eq.(15).

$$c_{k\neq i}^{(1)} = \frac{{\boldsymbol{\psi}_i^{(0)}}^T\boldsymbol{F}_i^{(1)}}{{w_k^{(0)}}^2 - {w_i^{(0)}}^2} \tag{15}$$

If $i = k$, Eq.(15) cannot be evaluated. The coefficients $c_{k=i}^{(1)}$ have to be determined by other means. A second convenient normalization, given by Eq.(16), is considered. Instead of directly considering a perturbed mass normalization homogeneous to Eq.(9), this equation links the 0^{th} order eigenvector $\boldsymbol{\psi}_i^{(0)}$ and the high

order eigenvector $\boldsymbol{\psi}_i$ to the full mass matrix. The aim is to limit the complexity of the following developments and use the orthonormal property of Eq.(9).

$$\boldsymbol{\psi}_i^{(0)^T} \mathbf{M} \boldsymbol{\psi}_i = 1 \tag{16}$$

Introducing Eq.(4) and Eq.(6) in Eq.(16) and keeping only the 1^{st} order terms, Eq.(17) reads as :

$$\boldsymbol{\psi}_i^{(0)^T} \mathbf{M}_S \boldsymbol{\psi}_i^{(1)} + \boldsymbol{\psi}_i^{(0)^T} \mathbf{M}_A \boldsymbol{\psi}_i^{(0)} = 0 \tag{17}$$

Substituting the 1^{st} order eigenvector by the linear combination given by Eq.(13) and considering that normal modes are $\mathbf{M}_S$ orthonormals, the $c_{k=i}^{(1)}$ coefficient can be calculated with Eq.(18).

$$c_{k=i}^{(1)} = -\boldsymbol{\psi}_i^{(0)^T} \mathbf{M}_A \boldsymbol{\psi}_i^{(0)} \tag{18}$$

3.4. Identification of the n^{th} order terms

Following the developments detailed in section 3.3, expressions to evaluate any n^{th} order of the i^{th} eigensolutions can be determined and are given by Eq.(19) to Eq.(25).

$$\left(\mathbf{K}_S + s_i^{(0)^2} \mathbf{M}_S\right) \boldsymbol{\psi}_i^{(n)} = \mathbf{F}_i^{(n)} \tag{19}$$

where

$$\mathbf{F}_i^{(n)} = -\left(2 s_i^{(0)} \mathbf{M}_S \boldsymbol{\psi}_i^{(0)}\right) s_i^{(n)} - \mathbf{G}_i^{(n)} \tag{20}$$

$$\begin{aligned} \mathbf{G}_i^{(n)} = {} & \mathbf{K}_A \boldsymbol{\psi}_i^{(n-1)} + \mathbf{C}_A \sum_{k=0}^{n-1} \boldsymbol{\psi}_i^{(k)} s_i^{(n-k-1)} + \mathbf{M}_A \left(\sum_{k=0}^{n-1} \left(\sum_{l=0}^{n-1-k} s_i^{(l)} s_i^{(n-k-l-1)} \right) \boldsymbol{\psi}_i^{(k)} \right) \\ & + 2\mathbf{M}_S \left[\sum_{k=1}^{n-1} s^{(0)} s_i^{(k)} \boldsymbol{\psi}_i^{(n-k)} + \mathbb{1}_{\{n \geq 3\}} \sum_{l=1}^{\lfloor \frac{n}{2} \rfloor - mod((n+1),2)} \left(\sum_{k=l+1}^{n-l} \left(s_i^{(l)} s_i^{(k)} \boldsymbol{\psi}_i^{(n-k-l)} \right) \right) \right] \\ & + \mathbf{M}_S \left(\sum_{k=1}^{\lfloor \frac{n}{2} \rfloor} s_i^{(k)^2} \boldsymbol{\psi}_i^{(n-2k)} \right) \end{aligned} \tag{21}$$

where $mod(x, 2)$ is the modulo 2 of x, $\lfloor x \rfloor$ corresponds to the greatest integer less than or equal to x, also denoted floor(x) and where the indicator function $\mathbb{1}_{\{n \geq p\}}$ equals 1 if n is superior to p and 0 otherwise.

$$s_i^{(n)} = \frac{-\boldsymbol{\psi}_i^{(0)^T} \mathbf{G}_i^{(n)}}{2 s_i^{(0)}} \tag{22}$$

$$\begin{aligned} \boldsymbol{\psi}_i^{(n)} &= \sum_{k=1}^{m} c_k^{(n)} \boldsymbol{\psi}_k^{(0)} + \boldsymbol{\Gamma}_i^{(n)} \\ \Gamma_i^{(n)} &= \mathbf{K}_S^{-1} \mathbf{F}_i^{(n)} - \sum_{k=1}^{m} \frac{\boldsymbol{\psi}_k^{(0)^T} \boldsymbol{F}_i^{(n)}}{\omega_k^{(0)^2}} \boldsymbol{\psi}_i^{(0)} \end{aligned} \tag{23}$$

$$c_{k\neq i}^{(n)} = \frac{{\boldsymbol{\psi}_i^{(0)}}^T \boldsymbol{F}_i^{(j)}}{\omega_k^{(0)^2} - \omega_i^{(0)^2}} \tag{24}$$

$$c_{k=i}^{(n)} = -{\boldsymbol{\psi}_i^{(0)}}^T \mathbf{M}_A \boldsymbol{\psi}_i^{(n-1)} \tag{25}$$

The computation of perturbed eigensolutions has to solve a linear system of size N (Eq.(14) or Eq.(23)) for each mode which can be time consuming for large systems. However the symmetric contribution of the stiffness matrix involved in these expressions can be decomposed once to minimize the additional computational cost.

3.5. Construction of the projection basis

With the classical method, the projection basis $\mathbf{T}$ is built with nm normal modes of Eq.(2), such as :

$$\mathbf{T} = [\boldsymbol{\phi}_1 \ \dots \ \boldsymbol{\phi}_{nm}] \tag{26}$$

Since this basis is obtained with the associated conservative system's solutions, the subspace contains no information of damping nor any matrix asymmetric contributions. Thus, the key idea of the suggested method is to integrate damping and asymmetric information into the projection basis with additional order modes calculated from HPM. In a sense, the suggested method, further named HOPEP in this paper, retains the same characteristics of the classical method for large problems, namely linearization of the QEP, projection to reduce the corresponding GEP and then resolution with a global algorithm. HOPEP can then be considered as a generalization of the classical method.

Consequently, the projection basis $\mathbf{T}$ in HOPEP takes the following form :

$$\mathbf{T} = \left[\boldsymbol{\phi}_1^{(0)} \ \dots \ \boldsymbol{\phi}_{nm}^{(0)} \ \boldsymbol{\psi}_1^{(1)} \ \dots \ \boldsymbol{\psi}_m^{(d)}\right] \tag{27}$$

where m is the number of complex perturbed modes at each order. It is worth noting that the same number of normal modes is retained in expansions Eq.(14) and Eq.(23). This solution guarantees a constant number of normal modes for the computation of the perturbed modes during the iterations of the HOPEP algorithm. Several tests have also shown that increasing the number of normal modes did not significantly improve the results.

When dealing with complex values in a numerical analysis, it is common practice to separate the real and imaginary parts of mathematical expressions. This solution allows the preservation of as much information as possible but doubles the number of modes in the projection basis, and therefore the time to solve the QEP. A more economic solution considers only the real parts of perturbed eigenvectors. It is important however to keep sufficient information in the real part before decomposing complex quantities. It is a common practice [38] to scale the complex matrix with the maximum value in each column and retain only the modified real part.

As the projection basis $\mathbf{T}$ in HOPEP is composed of a set of modes from different types or orders, it is mandatory to proceed with orthonormalization phase. Here, two numerical methods have been identified. The first method is the so-called iterative Gram-Schmidt process [39]. This method is very accurate and allows for the computation of an orthormal basis preserving the initial size. The second method, implemented in the Structural Dynamics Toolbox [40], orthonormalizes the projection basis using a preconditioned Cholesky decomposition and eliminates possible collinear vectors using a singular value decomposition. An advantage of this second solution is a lower numerical cost. For both methods, vectors of the basis are normalized thanks to the identity matrix.

Once the different calculations detailed above have been performed, the modified projection basis $\mathbf{T}$ is used in Eq.(3) to solve approximate solutions of the QEP.

Many tests have shown that HOPEP's performance relies on a good balance between the number of normal modes, the number of perturbed eigenvectors and the maximum homotopy order. The flowchart in Fig. 1 depicts a strategy to efficiently build the projection basis. The algorithm mainly focuses on the sequence and criteria used to define the number of normal modes and the maximum homotopy order. Indeed, the number of perturbed eigenvectors (m) is fixed to the number of mode of interest since a stabilization of all complex eigensolutions is required in the entire frequency band. It is worth noting that every change in the projection basis is followed by a new evaluation of the QEP.

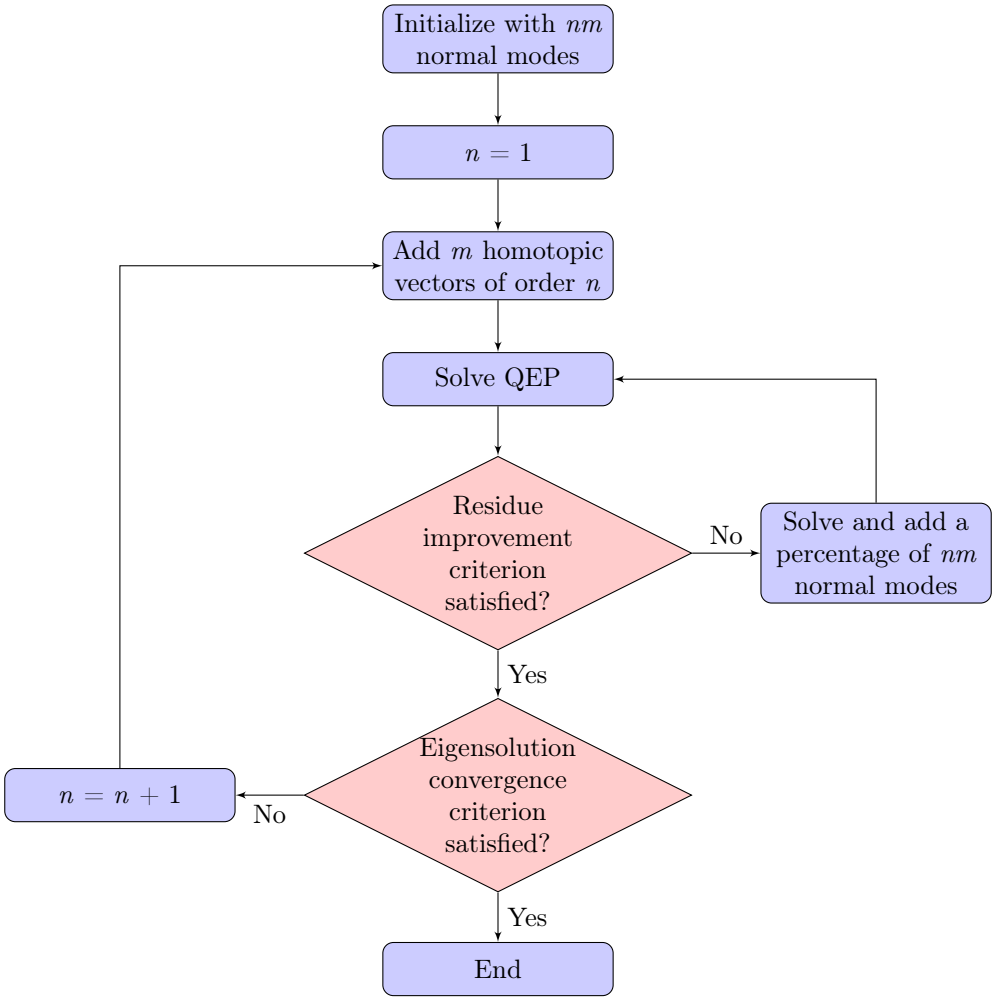

Figure 1: Construction of the projection basis.

Starting with several normal modes equals to the number of modes in the frequency band of interest, additional normal modes or homotopy orders are iteratively added to the projection basis. The process is achieved by monitoring the evolution of the residual error and the convergence of eigensolutions. For each mode, the residual error is calculated using the Manhattan norm of the residual vector defined by Eq.(28):

$$R_i = \| \left(\mathbf{K} + s_i^* \mathbf{C} + s_i^{*2} \mathbf{M} \right) \boldsymbol{\psi}_i^* \|_1 \tag{28}$$

It is expected that perturbed eigenvectors of any order added to the projection basis, will reduce the residual errors for all complex modes compared to those calculated at order 0. However, in practice, it is more relevant to first increase the number of normal modes rather than homotopy order if the residual error is not reduced for all modes, or at least a large number of them. It is important to note that an increase in normal modes has no effect on perturbed eigenvectors previously calculated since they required only the first m normal modes in Eq.(14) or Eq.(23). Perturbed eigenvectors already calculated can thus be stored and reused. The convergence criterion is evaluated using the relative errors between eigensolutions of two successive orders. In practice, it is sufficient to monitor only the real parts of eigensolutions. The algorithm stops when relative errors for all modes of interest are inferior to a given threshold, otherwise a new homotopy order is added to the projection basis.

In the next section, the different projection basis configurations detailed above are studied in a finite element application dedicated to a friction-induced vibration problem.

4. Application of the HOPEP method

The stability of a brake system can be analyzed in the Lyapunov sense through the frequency method. This method involves performing a Complex Eigenvalue Analysis (CEA), in which the system of equations is linearised around a stationary state. Positive real parts of complex eigenvalues allow to state for unstable modes.

All tests performed on the brake model described in section 4.1 require a starting phase presented in section 4.2. Sections 4.3 and 4.4 analyse the effects of key parameters thanks to the convergence of complex eigensolutions and to the evolution of the residual error. The algorithm presented in section 3.5 is applied in section 4.5. In each case, the frequency band of interest is inferior to 20 kHz. In this frequency band, 74 complex modes are computed from the classical projection method.

For all tests, homotopy developments are limited to a $6^{th} order$ which represents a good balance between precision and numerical cost. Results are analysed thanks to the evolution of the QEP residues and relative errors on complex eigensolutions. For complex eigenvalues, standard formulations compare the real parts Eq.(29) and the natural circular frequencies Eq.(30), separately. The chosen relative error in complex eigenvectors, defined by Eq.(31), is of the most accurate since major errors in only one vector component are noticed. It is normal to consider that a value below 10% denotes a very good agreement. An eigenvector correlation is performed with the most widely used Modal Assurance Criterion (MAC), as recalled in Eq.(32) for complex quantities.

$$e_{Re(s_i)} = \frac{Re(s_i^{*(n+1)}) - Re(s_i^{*(n)})}{Re(s_i^{*(n+1)})} \tag{29}$$

$$e_{|s_i|} = \frac{|s_i^{*(n+1)}| - |s_i^{*(n)}|}{|s_i^{*(n+1)}|} \tag{30}$$

$$e_{\boldsymbol{\psi}_i} = \frac{\|\boldsymbol{\psi}_i^{*(n+1)} - \boldsymbol{\psi}_i^{*(n)}\|}{\|\boldsymbol{\psi}_i^{*(n+1)}\| + \|\boldsymbol{\psi}_i^{*(n)}\|} \tag{31}$$

$$MAC_{ik} = \frac{\|\boldsymbol{\psi}_i^{*(n+1)H} \boldsymbol{\psi}_k^{*(n)}\|^2}{\|\boldsymbol{\psi}_i^{*(n+1)H} \boldsymbol{\psi}_i^{*(n+1)}\| \|\boldsymbol{\psi}_k^{*(n)H} \boldsymbol{\psi}_k^{*(n)}\|} \tag{32}$$

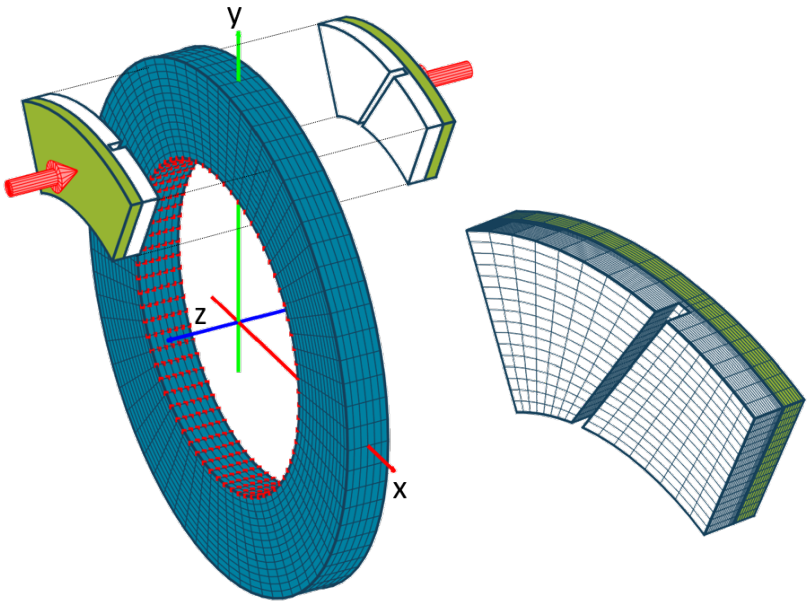

Figure 2: FE model of the simplified brake system.

4.1. Studied model

The case study is a simplified brake system composed of two pads and a disc. An exploded view of the brake FE model and a detailed view of a pad are depicted in Fig. 2.

Each pad is constituted of a lining with a centered diagonal slot and a back plate. The full mesh is composed of 23302 nodes and 19104 linear brick elements. The coupled model contains 66490 DOF. Material properties are cast iron for the disc, steel for the backplates and a sintered material for the linings.

Material behaviour of the disc and backplates is supposed isotropic but transverse isotropic material is considered for the linings. The dimensions and material properties of each component are reported in Table 1.

A Rayleigh damping has been chosen to model the damping of the three components. Mass and stiffness damping coefficients, namely α and β, as well as friction coefficient μ between pads and disc are reported in Table 2.

To complete the model description, fixed boundary conditions for all directions are applied on interior diameter nodes of the disc (the red markers in Fig. 2) and all translations along x and y are fixed for the pads. Moreover, a pressure of 25 bars, represented by the red arrows, is applied on the external pad surfaces and a rotation velocity of 8.17 rad/s around the z axis is applied to the disc to initiate sliding friction.

4.2. Preliminary computations

The FE model of the brake system is pre-computed in the commercial software Abaqus. The stiffness $\mathbf{K}_0$, damping $\mathbf{C}_0$ and mass $\mathbf{M}_0$ matrices of the uncoupled system (i.e bloc diagonal matrices) are exported in a dedicated software developed in Matlab. To initiate HOPEP calculations, symmetric and asymmetric decompositions of the matrices are computed using normal and tangential connectivity matrices $\mathbf{T}_N$ and $\mathbf{T}_f$ respectively together with Eq.(33) to Eq.(37) :

$$\mathbf{M}_S = \mathbf{T}_N^T \mathbf{M}_0 \mathbf{T}_N \tag{33}$$

Table 1
Geometrical and material parameters of the simplified brake model.

Component	**Parameter**	**Value**	**Unit**
Disc	Thickness	25.	mm
	Inner radius	95.5	mm
	Outer radius	152.5	mm
	Density	7200.	kg/m^3
	Young Modulus	130.	GPa
	Poisson's ratio (ν)	0.3	
Back plate	Thickness	7.	mm
	Inner radius	96.5	mm
	Outer radius	151.5	mm
	Angle	$2\pi/7$	radians
	Density	7300.	kg/m^3
	Young Modulus	170.	GPa
	Poisson's ratio (ν)	0.3	
Lining	Thickness	10.	mm
	Inner radius	96.5	mm
	Outer radius	151.5	mm
	Angle	$2\pi/7$	radians
	Slot width	5.	mm
	Density	2600.	kg/m^3
	Young Modulus (E_x)	6.5	GPa
	Young Modulus (E_z)	3.5	GPa
	Poisson's ratio (ν_{xy})	0.15	
	Poisson's ratio (ν_{xz})	0.20	
	Shear Modulus (G_{yz})	1.	GPa

Table 2
Friction and Rayleigh coefficients for the brake system.

Parameter	**Value**	**Unit**
Friction coefficient μ	0.6	
Damping coefficient α	25.	s^{-1}
Damping coefficient β	5.10^{-8}	s

$$\mathbf{M}_A = \mathbf{T}_f^T(\mu)\mathbf{M}_0\mathbf{T}_N - \mathbf{M}_S \tag{34}$$

$$\mathbf{K}_S = \mathbf{T}_N^T\mathbf{K}_0\mathbf{T}_N \tag{35}$$

$$\mathbf{K}_A = \mathbf{T}_f^T(\mu)\mathbf{K}_0\mathbf{T}_N - \mathbf{K}_S \tag{36}$$

$$\mathbf{C}_A = \mathbf{T}_f^T(\mu)\mathbf{C}_0\mathbf{T}_N \tag{37}$$

4.3. Influence of the projection basis arrangement

This first test shows the mutual influence of the number of normal modes and the homotopy order for the convergence of complex eigensolutions. In order to do this, three configurations of the projection basis are considered:

- a gradual increase of sets of normal modes (from nm to $7\times nm$)
- nm normal modes completed by sets of m perturbed eigenvectors up to order 6
- $2\times nm$ normal modes completed by sets of m perturbed eigenvectors up to order 6

For the three configurations, values of parameters nm and m are fixed to the number of complex modes of interest (nm=m=74). Perturbed eigenvectors are decomposed into real and imaginary parts and the projection basis is orthonormalized using the iterative Gram-Schmidt process in order to preserve all available information.

Fig. 3 shows the convergence evolutions of the eigensolutions namely, real part of eigenvalues, natural circular frequencies and eigenvector norms, as a function of two successive orders. Residual evolution is represented as a function of orders. It is worth noting that, for the first projection basis configuration, an order stands for a set of normal modes. As we would like to observe an improvement for all results in the frequency band of interest, convergence and residual evolutions are monitored by respectively the maximum relative errors and the maximum residual errors which are calculated for all modes.

The four graphs in Fig. 3 clearly show that the first configuration of the projection basis does not lead to improved results although more than five hundred normal modes are kept at the last order. The same remark applies to the second configuration. Perturbed eigenvectors have no effect when they are associated with the minimal number of normal modes. For the third projection basis configuration, where the number of normal modes is doubled, results are very interesting. In fact, in all cases the evolution of the three convergence criteria present the same decrease, attesting to the stabilization of solutions. The main improvement is observed for real parts and eigenvector norms where maximum relative errors calculated between order 0 and order 1 are relatively high denoting large discrepancies for some modes. Increasing the homotopy order significantly reduce these errors which can reach very low values for real parts. For example, reductions of

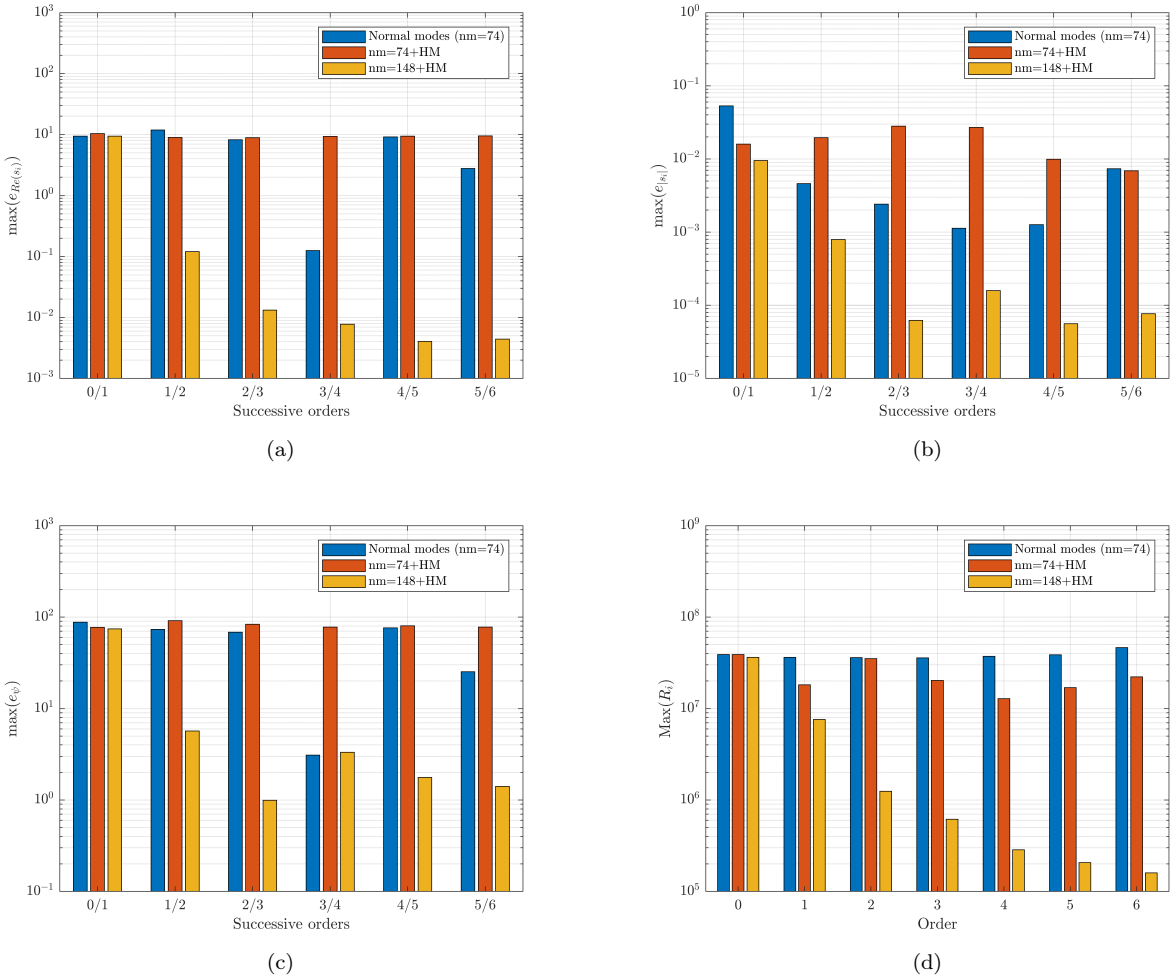

Figure 3: Influence of projection basis content. Evolution of errors as a function of homotopy orders for: (a) real parts; (b) natural circular frequencies; (c) complex eigenvector; (d) QEP residual.

two orders of magnitude are obtained with only two homotopy orders. For circular natural frequencies the maximum relative error is already low (below 1%) between order 0 and order 1 denoting a good evaluation of these quantities with the classical projection basis. The evolution of residual errors follows the same trend and confirms a gradual improvement in the QEP solving with increasing homotopy order.

In conclusion, these first results give us two main characteristics of the suggested method. Firstly, the use of perturbed eigenvectors efficiently improves the QEP solutions provided that the size of the normal modes basis is greater than the number of mode of interest. Secondly, the stabilization of QEP solutions can be monitored with only the real part of eigenvalues.

4.4. Influence of normalization scheme

The second test aims to study the influences of the orthonormalization scheme as well as the decomposition of complex perturbed eigenvectors using either real and imaginary parts (labelled R+I) or modified real parts (labelled Rm). The projection basis can be orthonormalized either with the Gram-Schmidt process (labelled GS) or with the Cholesky decomposition (labelled Chol). In all four cases, the configuration of the projection bases follows the best out of the previous test, namely a normal mode basis of 148 eigenvectors completed with sets of 74 perturbed eigenvectors up to order 6.

As before, Fig. 4 shows the maximum relative errors of the eigensolutions as a function of two successive homotopy orders and the maximum residual errors as a function of homotopy orders.

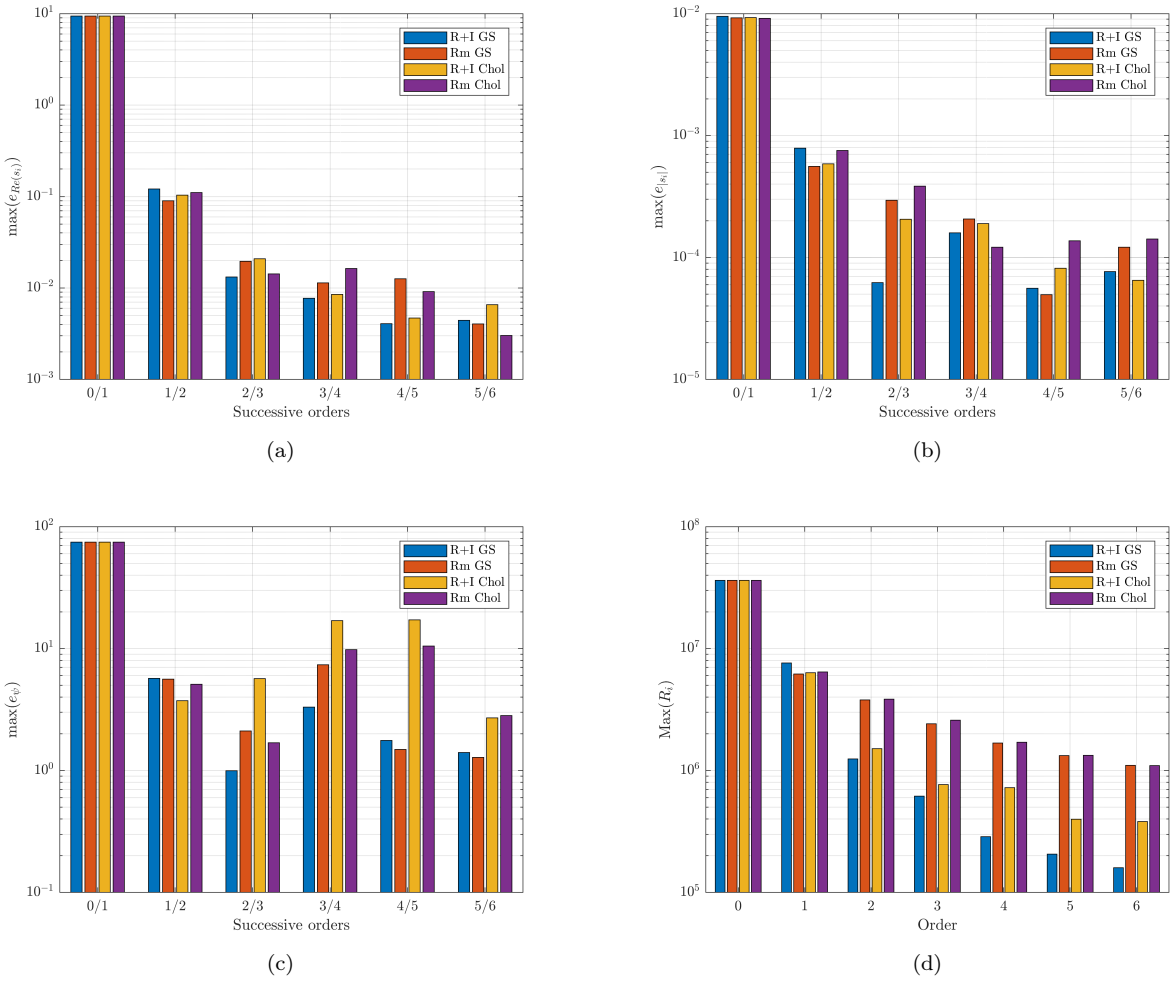

Figure 4: Influence of projection basis orthonormalization. Evolution of errors as a function of homotopy orders for: (a) real parts; (b) natural circular frequencies; (c) complex eigenvectors; (d) QEP residual.

Regarding the stabilization of eigensolutions, there is no significant difference between the four configurations meaning that the convergence of complex eigensolutions is not affected by the orthonormalization and the decomposition schemes. Regarding the evolution of the residual errors, the global trend is the same for all configurations with a reduction of errors as a function of homotopy order. The best configuration remains the one which uses the Gram-Schmidt process on the real and imaginary parts of perturbed eigenvectors. The main difference deals with the gap in residual errors values mainly due to the choice of the modified real part decomposition and in a lesser extent, to the Cholesky decomposition. However, in both cases the gap compared to the best configuration does not exceed half an order of magnitude. It is thus interesting to consider the modified real part decomposition for lower numerical cost reason. Indeed, in that case, the size of the projection basis is half the size of the other decomposition scheme.

4.5. Application of the HOPEP algorithm

In the HOPEP algorithm, the iterative construction of the projection basis relies on the residue criterion and the stabilization criterion which govern an increase of respectively the number of normal modes and of

the homotopy order. The residue criterion at order n is validated if the difference between the residual error at that order and the residual error at order 0 is negative. Ideally, this criterion should be validated for all complex modes. In practice, a reasonable threshold can be fixed to 95% of the number of modes. With the second criterion, solutions of the QEP are considered stabilized if relative errors between real parts of complex eigenvalues for two successive orders are inferior to a given threshold, typically 5%.

In this section, the behaviour of these two criteria is studied through three configurations of the projection basis. The first configuration corresponds to the initialization phase of the algorithm where the size of the normal mode basis is fixed to the nm=74 complex modes of interest. For the second configuration, the normal mode basis is chosen in a frequency band increased by 10% (up to 22 kHz) and contains nm=93 modes. In the same way, the frequency band for the third configuration is increased by 20% which provides a normal mode basis with nm=113 modes. For the three configurations the projection bases are progressively completed by the modified real part of perturbed eigenvectors up to order 6 and are orthonormalized thanks to the Gram-Schmidt process. We are interested by the 74 first complex modes of the QEP and the threshold for the stabilization criterion is fixed to 5%.

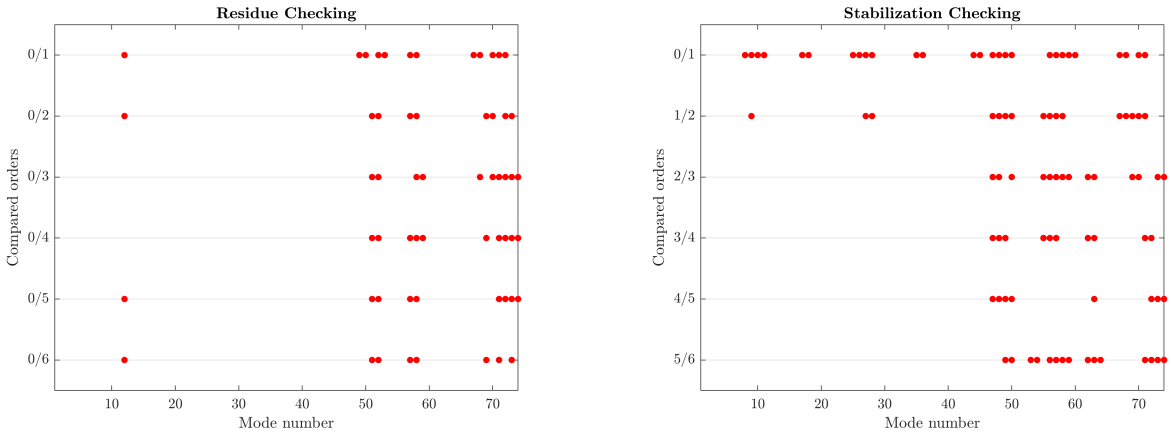

(a) (b)

Figure 5: (a) Residual criterion checking per mode and (b) stabilization criterion checking per mode as a function of homotopy orders for the first configuration (***nm*=74**). A red dot indicates an unsatisfactory check.

The results of the first configuration are reported in Fig. 5 with the progression of the homotopy order (from top to bottom). A red dot indicates that the residual improvement or the stabilization is not valid for the related mode. With this configuration, the normal mode basis is not sufficient to stabilize the complex modes in the higher frequency band and the residual error is not improved for 10% of modes, no matter what the homotopy order is.

In the same way, the results of the second configuration are presented in Fig. 6 and in Fig. 7 for the third configuration. In both cases, validations of the two criteria have notably improved. However, Fig. 6(b) shows that six homotopy orders are required to stabilize modes in the entire frequency band. We can also note that residual errors are improved for the majority of modes at each step of the iterative process. As expected with the third configuration, results again improved faster since three homotopy orders are enough to stabilize all modes.

Table 3 presents a focus on real parts and frequencies calculated with the three configurations from order 0 (normal modes only) up to order 3 in a way that shows the behaviour of the results according to the setting of the projection basis more specifically. In this table, positive values of real parts, which correspond to unstable modes, are highlighted in light gray. Apart from mode number 46 where results are stable, we can globally observe once again that real parts of eigenvalues are mainly affected, both in signs and in values.

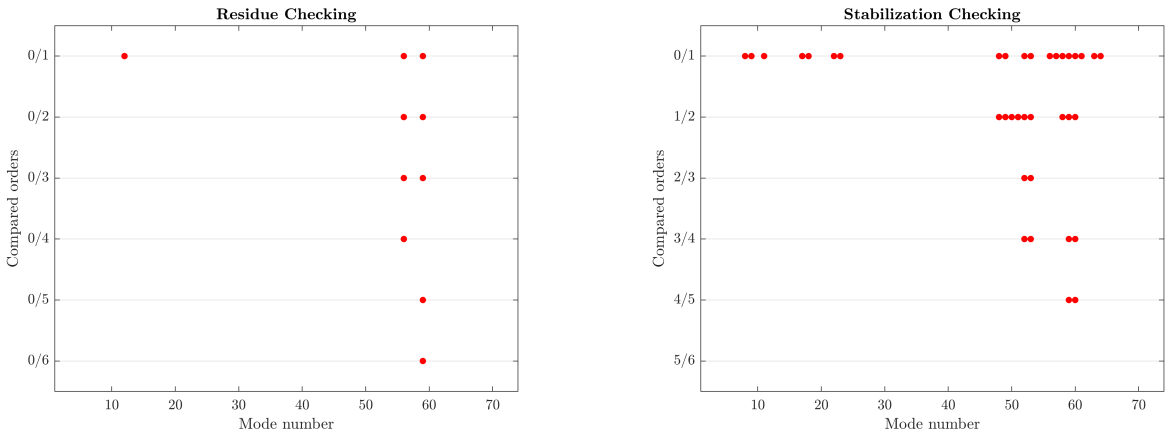

(a) (b)

Figure 6: (a) Residual criterion checking per mode and (b) stabilization criterion checking per mode as a function of homotopy orders for the second configuration (***nm*=93**). A red dot indicates an unsatisfactory check.

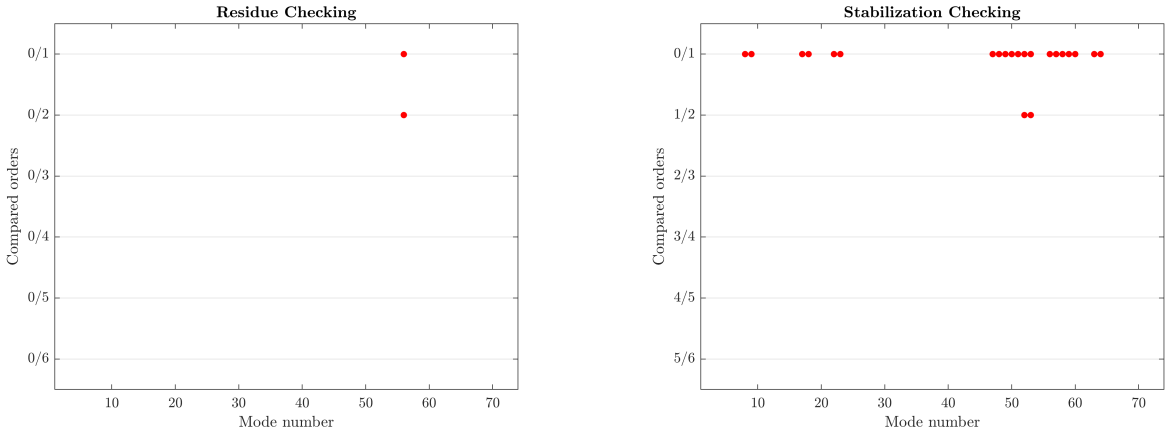

(a) (b)

Figure 7: (a) Residual criterion checking per mode and (b) stabilization criterion checking per mode as a function of homotopy orders for the third configuration (***nm*=113**). A red dot indicates an unsatisfactory check.

Important variations of real part values can be observed for modes number 47, 51 and 52 but they stabilized quickly with homotopy orders in the third configuration (nm=113).

For mode number 53 the real part is always negative for the first configuration (nm=74) indicating a stable mode. For the second (nm=93) and the third configurations, this real part becomes positive as soon as one homotopy order is taken into account but remains negative if only normal modes are considered. We can also observe that real parts and frequencies completely stabilize with three homotopy orders for the third configuration.

With regard to modes 48 to 50, important fluctuations of real parts are observed depending on the number of normal modes used in the projection basis. Regarding the first configuration, starting with three stable modes, two unstable modes are finally detected if homotopy orders are added. Nevertheless, large

variations of the values of the real parts lead to a doubtful perception of this result. On the other hand, for the second and the third configurations, the state of the modes is completely different since only the mode number 49 is detected as unstable. This situation clearly shows that the stability of the eigensolutions is governed by a good balance of normal modes and homotopy orders. Indeed, with the highest number of normal modes without homotopy order, modes number 48 and 50 would be considered as unstable. However, the amount of normal modes remains essential to improving the convergence of the stabilization as can be observed for the third configuration compared to the second one.

All observations given above are also strengthened by correlations and relative eigenvector errors reported in Table 4. Comparison between eigenvectors of the same number can be arguable because it can be seen that some MAC values, for modes 47 to 49, do not correspond to any agreement between modes shapes. There is no reference here and eigensolutions are then analyzed in the sense of convergence. One can observe a very good improvement in correlations and a drastic decrease in errors as soon as both normal mode number and homotopy orders increase. This is particularly true for the third configuration at order 3 where relative eigenvector errors are below 1% which denotes quasi identical vectors.

This test shows that the numerical cost can be reduced if the normal mode basis is increased first. This condition is controlled by the residual improvement at the first step of the algorithm and needs a reduction in residue for a large number of modes, 98% in that case. Moreover, if less normal modes are selected, simulations in the second configuration tell us that a better quality of complex eigensolutions can be obtained with higher homotopy orders. Consequently, for an application such as friction-induced vibration, the mode's stability status can be better evaluated.

5. Conclusion

In this study, an homotopy projection basis has been suggested as a generalization of the classical projection basis used to solve a QEP. The key idea with the HPM is here to consider the asymmetric parts of the mass and stiffness matrices and full damping matrix as non-linear parts of the problem. The development of perturbed eigensolutions is formulated in a way to reduce the numerical cost. An algorithm is also suggested to efficiently build a sufficient projection basis, again, minimizing the additional numerical cost. The numerical analyses clearly highlight that the new projection basis allows for the good stabilization of complex eigensolutions in the entire frequency band. Moreover, a significant reduction of QEP residue confirms the confidence of the results.

Acknowledgements

This work was carried out within the framework of the CNRS Research Federation on Ground Transports and Mobility, in association with the ELSAT2020 project supported by the European Community, the French Ministry of Higher Education and Research and the Hauts de France Regional Council. The authors gratefully acknowledge the support of these institutions.

References

[1] F. Tisseur, K. Meerbergen, The quadratic eigenvalue problem, SIAM Review 43 (2) (2001) 235–286. doi:10.1137/S0036144500381988.
URL https://doi.org/10.1137/S0036144500381988

[2] E. Balmès, Parametric families of reduced finite element models. theory and applications, Mechanical Systems and Signal Processing 10 (4) (1996) 381 – 394. doi:https://doi.org/10.1006/mssp.1996.0027.
URL http://www.sciencedirect.com/science/article/pii/S0888327096900278

[3] F. Massa, T. Tison, B. Lallemand, O. Cazier, Structural modal reanalysis methods using homotopy perturbation and projection techniques, Computer Methods in Applied Mechanics and Engineering 200 (45) (2011) 2971 – 2982. doi:https://doi.org/10.1016/j.cma.2011.06.016.
URL http://www.sciencedirect.com/science/article/pii/S0045782511002349

[4] S. Chen, X. Yang, H. Lian, Comparison of several eigenvalue reanalysis methods for modified structures, Structural and Multidisciplinary Optimization 20 (2000) 253 – 259.

Table 3
Real parts and natural frequencies for a selection of modes. Values are given for the three configurations of the projection basis from homotopy order 0 (H0) up to order 3 (H3).

Modes No	**Re**(s_i)	$\lvert s_i\rvert/2\pi$	**Re**(s_i)	$\lvert s_i\rvert/2\pi$	**Re**(s_i)	$\lvert s_i\rvert/2\pi$	**Re**(s_i)	$\lvert s_i\rvert/2\pi$
	***nm*=74 H0**		***nm*=74 H1**		***nm*=74 H2**		***nm*=74 H3**	
46	-297.78	17001.38	-298.71	17029.26	-299.34	17047.79	-299.19	17043.26
47	-319.65	17641.22	-1427.77	17924.99	-1731.21	17996.67	-1441.13	18077.99
48	-321.24	17686.83	768.63	17925.94	1067.05	17997.88	771.11	18078.95
49	-331.27	17971.80	-1246.17	18003.58	-1825.61	18089.39	-1929.98	18101.83
50	-333.28	18028.20	581.42	18004.37	1154.87	18090.68	1258.38	18103.22
51	-338.68	18179.48	-338.65	18178.50	-338.61	18177.42	-338.51	18174.75
52	-338.91	18185.70	-338.99	18188.03	-339.06	18189.92	-339.44	18200.59
53	-359.81	18758.83	-355.64	18646.06	-351.56	18534.85	-350.79	18513.63
	***nm*=93 H0**		***nm*=93 H1**		***nm*=93 H2**		***nm*=93 H3**	
46	-298.17	17012.97	-298.78	17031.24	-299.09	17040.34	-299.06	17039.61
47	-322.16	17712.98	-327.70	17870.91	-333.02	18020.99	-333.46	18033.21
48	-1431.20	17995.62	-1646.37	18077.69	-1792.70	18099.79	-1846.34	18110.00
49	767.05	17996.57	976.42	18078.83	1121.21	18101.06	1174.13	18111.31
50	-398.73	18180.62	-400.09	18179.11	-427.55	18169.97	-421.89	18170.66
51	-278.72	18180.67	-277.25	18179.16	-249.14	18170.05	-254.85	18170.73
52	-347.09	18412.20	-1852.22	18437.30	-1375.01	18385.26	-1759.76	18380.07
53	-350.84	18515.19	1156.40	18438.63	682.86	18386.17	1068.07	18381.32
	***nm*=113 H0**		***nm*=113 H1**		***nm*=113 H2**		***nm*=113 H3**	
46	-298.51	17023.16	-298.79	17031.55	-299.06	17039.46	-299.05	17039.33
47	-1712.34	18024.67	-335.06	18078.15	-334.78	18070.33	-334.70	18068.11
48	1046.19	18025.87	-1882.10	18092.98	-1862.89	18104.09	-1879.42	18109.32
49	-972.06	18070.48	1211.12	18094.33	1191.11	18105.42	1207.27	18110.66
50	302.51	18071.03	-429.02	18166.02	-427.42	18168.34	-424.84	18168.38
51	-338.37	18170.82	-247.38	18166.10	-249.15	18168.42	-251.73	18168.46
52	-339.79	18210.32	-1763.65	18354.98	-1900.46	18358.83	-1913.93	18357.78
53	-353.23	18580.28	1073.78	18356.23	1210.35	18360.20	1223.90	18359.17

[5] U. Kirsch, M. Bogomolni, I. Sheinman, Nonlinear dynamic reanalysis of structures by combined approximations, Computer Methods in Applied Mechanics and Engineering 195 (33) (2006) 4420 – 4432. doi:https://doi.org/10.1016/j.cma.2005.09.013.
URL http://www.sciencedirect.com/science/article/pii/S0045782505004391

[6] L. Ma, S. H. Chen, G. W. Meng, Combined approximation for reanalysis of complex eigenvalues, Computers and Structures 87 (7) (2009) 502 – 506. doi:https://doi.org/10.1016/j.compstruc.2009.01.009.
URL http://www.sciencedirect.com/science/article/pii/S0045794909000285

[7] H. Jian-jun, C. Xiang-zi, X. Bin, Structural modal reanalysis for large, simultaneous and multiple type modifications, Mechanical Systems and Signal Processing 62-63 (2015) 207 – 217. doi:https://doi.org/10.1016/j.ymssp.2015.03.019.
URL http://www.sciencedirect.com/science/article/pii/S0888327015001454

[8] N. Damil, M. Potier-Ferry, A. Najah, R. Chari, H. Lahmam, An iterative method based upon Padé approximants, Communications in Numerical Methods in Engineering 15 (10) (1999) 701–708. doi:10.1002/(SICI)1099-0887(199910)15:10<701::AID-CNM283>3.0.CO;2-L.

[9] A. Elhage-Hussein, M. Potier-Ferry, N. Damil, A numerical continuation method based on Padé approximants, International Journal of Solids and Structures 37 (46) (2000) 6981 – 7001. doi:https://doi.org/10.1016/S0020-7683(99)00323-6.
URL http://www.sciencedirect.com/science/article/pii/S0020768399003236

[10] J.-H. He, Homotopy perturbation technique, Computer Methods in Applied Mechanics and Engineering 178 (3) (1999) 257 – 262. doi:https://doi.org/10.1016/S0045-7825(99)00018-3.
URL http://www.sciencedirect.com/science/article/pii/S0045782599000183

[11] L. Duigou, E. M. Daya, M. Potier-Ferry, Iterative algorithms for non-linear eigenvalue problems. application to vibrations of viscoelastic shells, Computer Methods in Applied Mechanics and Engineering 192 (11) (2003) 1323 – 1335. doi:https://doi.org/10.1016/S0045-7825(02)00641-2.
URL http://www.sciencedirect.com/science/article/pii/S0045782502006412

Table 4
MAC and relative eigenvector errors for a selection of modes. Comparison results are given for three following homotopy order (H0-H1) to (H2-H3) of the three projection basis configurations.

Modes No	***MAC*** (%)	e_ψ(%)	***MAC*** (%)	e_ψ(%)	***MAC*** (%)	e_ψ(%)
i-k	***nm*=74 H0-H1**		***nm*=74 H1-H2**		***nm*=74 H2-H3**	
46-46	91.	15.34	98.	6.90	100.	1.34
47-47	85.	20.20	97.	8.81	99.	6.20
48-48	0.	70.31	97.	8.81	99.	6.20
49-49	4.	63.59	97.	9.36	100.	3.22
50-50	91.	15.23	97.	9.36	100.	3.22
51-51	99.	5.33	98.	8.57	97.	17.05
52-52	95.	16.26	97.	14.84	94.	27.45
53-53	94.	12.40	97.	9.31	100.	1.80
	***nm*=93 H0-H1**		***nm*=93 H1-H2**		***nm*=93 H2-H3**	
46-46	97.	11.04	100.	4.02	100.	0.69
47-47	1.	11.32	100.	9.30	100.	2.61
48-48	72.	8.41	100.	8.14	100.	3.03
49-49	0.	8.41	100.	8.14	100.	3.03
50-50	97.	27.63	100.	42.86	100.	4.82
51-51	97.	27.63	100.	42.86	100.	4.82
52-52	95.	14.20	100.	5.89	100.	6.16
53-53	92.	16.74	100.	5.89	100.	6.16
	***nm*=113 H0-H1**		***nm*=113 H1-H2**		***nm*=113 H2-H3**	
46-46	97.	8.31	100.	2.27	100.	0.51
47-47	1.	67.79	100.	1.03	100.	0.38
48-48	72.	27.41	100.	1.48	100.	0.61
49-49	0.	69.88	100.	1.48	100.	0.61
50-50	97.	14.85	100.	3.15	100.	0.72
51-51	97.	24.93	100.	3.15	100.	0.72
52-52	95.	12.54	100.	1.51	100.	0.39
53-53	92.	14.14	100.	1.51	100.	0.39

[12] F. Boumediene, J.-M. Cadou, L. Duigou, E. M. Daya, A reduction model for eigensolutions of damped viscoelastic sandwich structures, Mechanics Research Communications 57 (2014) 74 – 81. doi:https://doi.org/10.1016/j.mechrescom.2014.03.001.
URL http://www.sciencedirect.com/science/article/pii/S0093641314000263

[13] X. Sun, L. Du, V. Yang, A homotopy method for determining the eigenvalues of locally or non-locally reacting acoustic liners in flow ducts, Journal of Sound and Vibration 303 (1) (2007) 277 – 286. doi:https://doi.org/10.1016/j.jsv.2007.01.020.
URL http://www.sciencedirect.com/science/article/pii/S0022460X07000661

[14] M. K. Lee, M. H. Fouladi, S. N. Namasivayam, Natural frequencies of thin rectangular plates using homotopy-perturbation method, Applied Mathematical Modelling 50 (2017) 524 – 543. doi:https://doi.org/10.1016/j.apm.2017.05.050.
URL http://www.sciencedirect.com/science/article/pii/S0307904X17303906

[15] B. Claude, L. Duigou, G. Girault, J.-M. Cadou, Eigensolutions to a vibroacoustic interior coupled problem with a perturbation method, Comptes Rendus Mécanique 345 (2) (2017) 130 – 136. doi:https://doi.org/10.1016/j.crme.2016.11.002.
URL http://www.sciencedirect.com/science/article/pii/S1631072116301279

[16] B. Claude, L. Duigou, G. Girault, Y. Guevel, J. Cadou, Numerical comparison of eigenvalue algorithms for vibroacoustic problems, Mechanics Research Communications 91 (2018) 39 – 45. doi:https://doi.org/10.1016/j.mechrescom.2018.05.007.
URL http://www.sciencedirect.com/science/article/pii/S0093641318301964

[17] B. Claude, L. Duigou, G. Girault, J. Cadou, Study of damped vibrations of a vibroacoustic interior problem with viscoelastic sandwich structure using a high order newton solver, Journal of Sound and Vibration 462 (2019) 114947. doi:https://doi.org/10.1016/j.jsv.2019.114947.
URL http://www.sciencedirect.com/science/article/pii/S0022460X19305097

[18] G. Sliva, A. Brezillon, J. Cadou, L. Duigou, A study of the eigenvalue sensitivity by homotopy and perturbation methods, Journal of Computational and Applied Mathematics 234 (7) (2010) 2297 – 2302, fourth International Conference on Advanced COmputational Methods in ENgineering (ACOMEN 2008). doi:https://doi.org/10.1016/j.cam.2009.08.086.
URL http://www.sciencedirect.com/science/article/pii/S0377042709005664

[19] L. Li, Y. J. Hu, X. L. Wang, Modal modification of damped asymmetric systems without using the left eigenvectors, in: Mechanical Design and Power Engineering, Vol. 490 of Applied Mechanics and Materials, Trans Tech Publications Ltd, 2014, pp. 331–335. doi:10.4028/www.scientific.net/AMM.490-491.331.
[20] F. Massa, B. Lallemand, T. Tison, Multi-level homotopy perturbation and projection techniques for the reanalysis of quadratic eigenvalue problems: The application of stability analysis, Mechanical Systems and Signal Processing 52-53 (2015) 88 – 104. doi:https://doi.org/10.1016/j.ymssp.2014.07.013.
URL http://www.sciencedirect.com/science/article/pii/S0888327014002556
[21] H. Do, F. Massa, T. Tison, B. Lallemand, A global strategy for the stability analysis of friction induced vibration problem with parameter variations, Mechanical Systems and Signal Processing 84 (2017) 346 – 364. doi:https://doi.org/10.1016/j.ymssp.2016.07.029.
URL http://www.sciencedirect.com/science/article/pii/S0888327016302527
[22] F. Massa, I. Turpin, T. Tison, From homotopy perturbation technique to reduced order model for multiparametric modal analysis of large finite element models, Mechanical Systems and Signal Processing 96 (2017) 291 – 302. doi:https://doi.org/10.1016/j.ymssp.2017.04.025.
URL http://www.sciencedirect.com/science/article/pii/S0888327017302212
[23] C. B. Moler, G. W. Stewart, An algorithm for generalized matrix eigenvalue problems, SIAM Journal on Numerical Analysis 10 (2) (1973) 241–256. doi:10.1137/0710024.
URL https://doi.org/10.1137/0710024
[24] Y. Cherruault, G. Adomian, Decomposition methods: A new proof of convergence, Mathematical and Computer Modelling 18 (12) (1993) 103 – 106.
[25] J.-H. He, Variational iteration method – a kind of non-linear analytical technique: some examples, International Journal of Non-Linear Mechanics 34 (4) (1999) 699 – 708.
[26] S.-Q. Wang, J.-H. He, Variational iteration method for solving integro-differential equations, Physics Letters A 367 (3) (2007) 188 – 191.
[27] J.-H. He, Homotopy perturbation technique, Computer Methods in Applied Mechanics and Engineering 178 (3) (1999) 257 – 262.
[28] H. Vazquez-Leal, Generalized homotopy method for solving nonlinear differential equations, Computational and Applied Mathematics 33 (1) (2014) 275 – 288.
[29] C. K. Chen, S. H. Ho, Solving partial differential equations by two-dimensional differential transform method, Applied Mathematics and Computation 106 (2) (1999) 171 – 179.
[30] J.-H. He, A short review on analytical methods for a fully fourth-order nonlinear integral boundary value problem with fractal derivatives, International Journal of Numerical Methods for Heat and Fluid Flow (2020). doi:https://doi.org/10.1108/HFF-01-2020-0060.
[31] J.-H. He, X. Jin, A short review on analytical methods for the capillary oscillator in a nanoscale deformable tube, Mathematical Methods in the Applied Sciences (2020). doi:https://doi.org/10.1002/mma.6321.
[32] J.-H. He, A coupling method of a homotopy technique and a perturbation technique for non-linear problems, International Journal of Non-linear Mechanics 35 (2000) 37–43.
[33] J.-H. He, New interpretation of homotopy perturbation method, International Journal of Modern Physics B 20 (2006).
[34] J.-H. He, Homotopy perturbation method with two expanding parameters, Indian Journal of Physics 88 (2) (2014) 193–196.
[35] D.-N. Yu, J.-H. He, A. G. Garcıa, Homotopy perturbation method with an auxiliary parameter for nonlinear oscillators, Journal of Low Frequency Noise, Vibration and Active Control 38 (3-4) (2019) 1540–1554.
[36] J.-H. He, The simpler, the better: Analytical methods for nonlinear oscillators and fractional oscillators, Journal of Low Frequency Noise, Vibration and Active Control 38 (3-4) (2019) 1252–1260.
[37] B. P. Wang, Improved approximate methods for computing eigenvector derivatives in structural dynamics, AIAA Journal 29 (6) (1991) 1018–1020. arXiv:https://doi.org/10.2514/3.59945, doi:10.2514/3.59945.
URL https://doi.org/10.2514/3.59945
[38] U. Fuellekrug, Computation of real normal modes from complex eigenvectors, Mechanical Systems and Signal Processing 22 (1) (2008) 57 – 65. doi:https://doi.org/10.1016/j.ymssp.2007.07.009.
URL http://www.sciencedirect.com/science/article/pii/S088832700700115X
[39] R. Jamai, N. Damil, Influence of iterated Gram–Schmidt orthonormalization in the asymptotic numerical method, Comptes Rendus Mécanique 331 (5) (2003) 351 – 356. doi:https://doi.org/10.1016/S1631-0721(03)00072-X.
URL http://www.sciencedirect.com/science/article/pii/S163107210300072X
[40] E. Balmès, Structural Dynamics Toolbox (for use with MATLAB), February 24, 2019.